transfected it into neocortical primary neurons that had been cultured for 8 days, and 2 days later we detected the EGFP fluorescent signal in neurons (Fig. 4d). These findings suggested that the ATG sequence at position −77 functions as a translational start codon in neurons.

Finally, we cloned the entire novel *Shank3* transcript by using the RT-PCR method and an In10-F primer and a reverse primer within the 3′-untranslated region (UTR) (3UTR-R) and detected a PCR product of about 5 kb. Sequence analysis confirmed that this PCR product completely matched the spliced *Shank3* transcript from exon 11 to exon 22 (Fig. 5). As shown in Figure 2c the expression profile of this transcript in the developing brain was similar to the expression profile of 441 bp of the PCR product (Fig. 5a). Notably, the level of expression of this transcript at P14 was lower than that at P7 and P21. We also detected other transcripts of different sizes (about 3 kb), especially at P7 and P14 (Fig. 5a), and sequence analysis identified one of the PCR products as the transcript that lacked the sequence coded by exon 21. Since the transcript caused a frameshift in ligation with exon 20 to exon 22, it may produce the carboxyl-terminus truncated isoform that lacked a homer-binding region, a cortactin-binding region and an SAM (Fig. 5b). These findings indicated the existence of two different *Shank3* transcripts whose transcriptional initiation site is located in intron 10.

In the recent review by Jiang and Ehlers, the *Shank3c* transcripts are expressed under the control of promoter 3 located in intron 10 (Jiang and Ehlers 2013), and Wang and coworkers have identified two *Shank3c* transcripts (*Shank3c-1* and *Shank3c-2*; GenBank HQ405757 and HQ405758) (Wang *et al.* 2011). We therefore designated the novel *Shank3* transcripts found in this study *Shank3c-3* (a completely spliced form from exon 11 to exon 22; GenBank AB841411) and *Shank3c-4* (deletion of exon 21; GenBank AB841412).

### Expression profile of the novel SHANK3c isoforms in the developing mouse neocortex

We next investigated the expression of the novel SHANK3c isoforms in the developing mouse neocortex by an immunoblot analysis. First, we constructed three expression vectors that produce the myc-tagged SHANK3 isoforms, SHANK3a (full-length SHANK3), SHANK3c-3 and SHANK3c-4, transfected them into HEK293 cells, and determined the molecular size of the SHANK3 isoforms by immunoblot analysis with anti-myc antibody. As shown in Figure 6a, the SHANK3 isoforms had their expected molecular sizes: myc-SHANK3a consisted of 1730 amino acids (aa) plus 22 extra sequences aa that included myc-tag, myc-SHANK3c-3 of 1322 SHANK3c-3 aa plus 22 aa, and myc-SHANK3c-4 of 382 SHANK3c-4 aa plus 22 aa. Since the anti-Shank3 antibody we used recognizes the peptides coded within exon 21 (Uchino *et al.* 2006), myc-SHANK3c-4 was not detected by immunoblotting with anti-Shank3 antibody. Next, we identified the immunoblot bands that corresponded to the SHANK3a and SHANK3c-3 isoforms based on their molecular sizes (Fig. 6b) and examined the expression profile of the SHANK3 isoforms in the developing neocortex (Fig. 6c). The results of the immunoblot analysis suggested that SHANK3a expression increased during development but that expression of SHANK3c-3 transiently decreased at P21. However, since we have not yet developed a specific antibody for SHANK3c, further study will be necessary to draw any conclusions about the expression profiles of the SHANK3 isoforms.

### Difference between the distribution of SHANK3c isoforms with and without the carboxyl terminus expressed in neocortical primary neurons

Since a cortactin-binding region and an SAM are essential for SHANK3 targeting to synapses and clustering (Boeckers

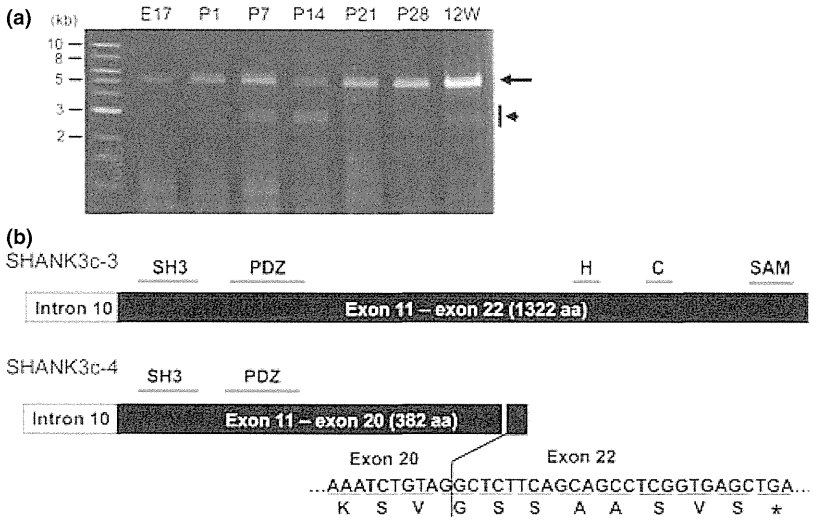


**Fig. 5** SHANK3 isoforms expressed from intron 10. (a) Representative agarose gel electrophoresis image showing expression of *Shank3* transcripts in the developing mouse neocortex. The arrow points to the *Shank3* transcript that contains exon 11 - exon 22, and the arrowhead points to the several alternative splicing variants. Size markers (1 kb ladder) are shown at the left. (b) Schematic structure of SHANK3c-3, the novel SHANK3 isoform with all exons from exon 11 to exon 22, and SHANK3c-4, its alternative splicing variant, which lacks exon 21. H, homer-binding region; C, cortactin-binding region.

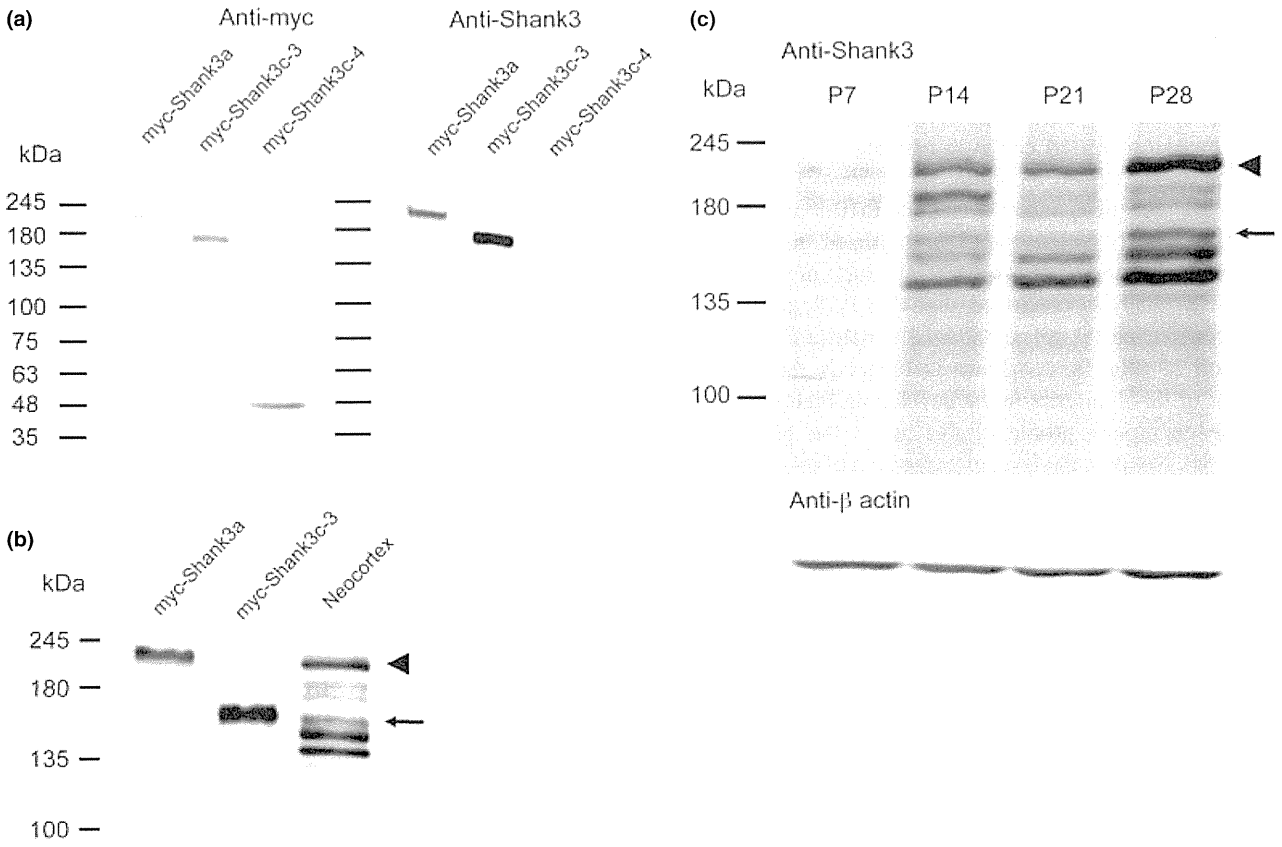


**Fig. 6** Expression profile of SHANK3c isoforms in the developing mouse neocortex. (a) Immunoblot analysis with anti-myc antibody (left panel) and anti-Shank3 antibody (right panel). Molecular weight standards are shown on the left. (b) Immunoblot analysis with anti-Shank3 antibody. A neocortical sample prepared from a mouse at P28 (50 μg) was loaded. The arrow indicates SHANK3c-3 and the arrowhead indicates SHANK3a. (c) Immunoblot analysis with anti-Shank3 antibody (upper panel) and anti-β actin (lower panel). Neocortical samples (50 μg) were loaded. The arrow indicates SHANK3c-3, and the arrowhead indicates SHANK3a.

*et al.* 2005), we examined the distribution of the carboxyl-terminus truncated SHANK3c-4 isoform that lacked the sequence coded by exon 21. We constructed two expression vectors carrying myc-tagged Shank3c-3 and Shank3c-4, whose translational start codon (ATG) is at position -77 in intron 10, under the CAG promoter (Fig. 3a, 5b, S2), and co-transfected each construct into neocortical primary neurons cultured for 9 days with the pCAGGS-EGFP plasmid to visualize the transfected neurons. After 7 days of culture, we fixed the cultured neurons and immunostained them with anti-myc antibody and anti-Shank3 antibody or anti-EGFP antibody. There was a close match between the immunoreactive signals obtained with anti-Shank3 antibody and anti-myc antibody in the transfected neurons (Fig. 7a). Judging from the morphology of the EGFP-positive neurites, the punctate expression signals of myc-Shank3c-3 were predominantly detected in the dendrites and few signals were detected in the axons (Fig. 7b). In contrast, the expression signals of myc-Shank3c-4 were diffusely observed in both the dendrites and axons (Fig. 7b). These results indicated that there is a large difference in synaptic localization between the two SHANK3c isoforms.

### MeCP2 binds the *Shank3* gene at the methylated CpG islands

To identify related molecules involved in expression of the novel *Shank3c* transcripts, we focused on MeCP2, which has been identified as the causative molecule of Rett syndrome and is thought to regulate gene transcription, mRNA splicing, and chromatin structure (Amir *et al.* 1999; Lam 2000; Hite *et al.* 2009). We investigated whether MeCP2 binds the methylated CpG islands of the *Shank3* gene by performing a ChIP assay. The results showed that at P1 MeCP2 bound CpG island-3 alone, but at P14 bound CpG island-2 and -4 in addition to CpG island-3 (Fig. 8). However, even though CpG island-5 was methylated the same as CpG island-4, no PCR product for CpG island-5 was detected even when two primer pairs were used (Fig. 8). No MeCP2 binding at CpG

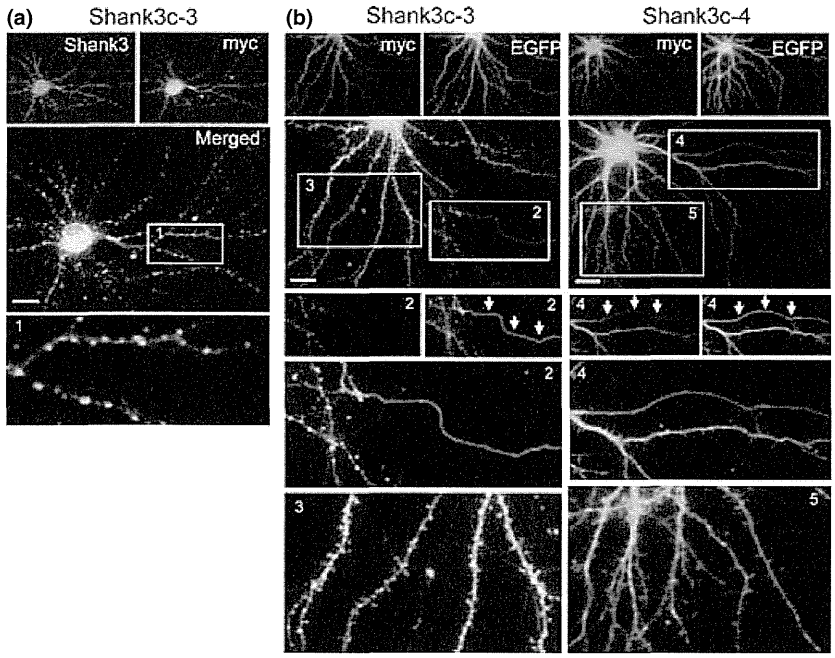


**Fig. 7** Difference between the distribution of SHANK3c isoforms with and without the carboxyl terminus expressed in neocortical primary neurons. Representative image of immunostained neurons. Neocortical primary neurons prepared from E15.5 mice were cultured for 9 days and co-transfected with pCAGGS-enhanced green fluorescent protein (EGFP) and the expression vector, pCAGGS-myc-Shank3c-3 or pCAGGS-myc-Shank3c-4. After culture for an additional 7 days cells were fixed and double-stained with anti-Shank3 antibody (red) and anti-myc antibody (green) (a) and with anti-myc antibody (red) and anti-enhanced green fluorescent protein (EGFP) antibody (green) (b). Enlarged images of each of the numbered boxes are shown. The arrows point to an axon. Scale bar shown in the merged images is 10 μm.

island-P, which was completely unmethylated at every stage of development tested, was detected at either P1 or P14 (data not shown).

### MeCP2 is involved in regulating expression of the novel *Shank3c* transcript

Next, we investigated the effect of MeCP2 on expression of the novel *Shank3c* transcripts. We prepared total RNA from neocortical tissue of *Mecp2*-deficient hemizygous male mice and wild-type littermates at the P7, P14, and P28 stages of development and performed a real-time RT-PCR. A previous electron-microscopic study revealed delayed neuronal development in *Mecp2*-deficient mice and that their nervous system contained numerous immature post-synaptic densities (Fukuda *et al.* 2005). First, we investigated expression of post-synaptic density-95 (PSD-95) (Fig. 9a). Although at P7 there were no significant differences in the level of PSD-95 expression between the *Mecp2*-deficient mice and wild-type mice, after P14 the level of PSD-95 expression in the *Mecp2*-deficient mice was significantly lower than in the wild-type mice, findings that were consistent with the results of a previous study that had indicated delayed neuronal development and abnormal synapses in *Mecp2*-deficient mice (wild-type mice: P14, 1.318 ± 0.020 (mean ± SEM) and P28, 1.152 ± 0.040; *Mecp2*-deficient mice: P7, 0.907 ± 0.030, P14, 1.017 ± 0.071, and P28, 0.856 ± 0.062). We then investigated the level of expression of two different *Shank3* transcripts in *Mecp2*-deficient mice: the *Shank3a* transcript, the major form of *Shank3* that is expressed from the 5′ end of the *Shank3* gene containing exon 1 (Fig. 9b), and the novel *Shank3c* transcript, whose transcriptional initiation site is located in intron 10 (Fig. 9c). During development, the level of *Shank3a* expression in the *Mecp2*-deficient mice was significantly lower than in the wild-type mice (wild-type mice: P14, 1.565 ± 0.030 and P28, 1.316 ± 0.020; *Mecp2*-deficient mice: P7, 0.896 ± 0.009, P14, 1.067 ± 0.011, and P28, 0.647 ± 0.005). In contrast, at P7 there was no significant difference between the levels of expression of the novel *Shank3c* transcript in intron 10 in the *Mecp2*-deficient mice and wild-type mice. However, at P14 expression of the novel *Shank3c* transcript in the *Mecp2*-deficient mice was clearly lower than in the wild-type mice (wild-type mice: P14, 0.824 ± 0.052 and P28, 1.654 ± 0.056; *Mecp2*-deficient mice: P7, 0.931 ± 0.049, P14, 0.547 ± 0.014, and P28, 1.480 ± 0.102). Interestingly, since at P28 the level of expression of the novel *Shank3* transcript in the *Mecp2*-deficient mice was not significantly different from its level of expression in the wild-type mice, the ratio of expression at

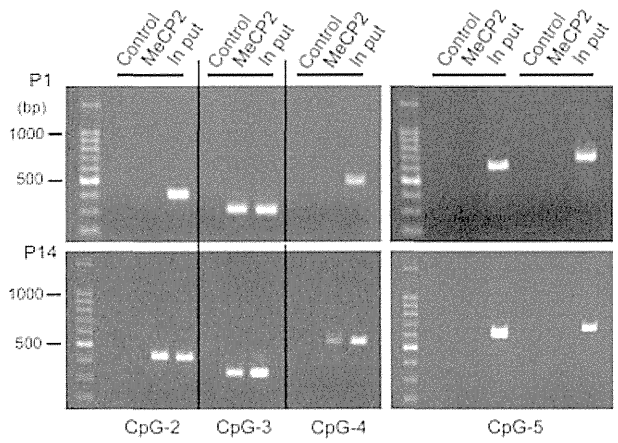


**Fig. 8** Chromatin immunoprecipitation assay of mouse neocortex at P1 and P14. Representative agarose gel electrophoresis image showing binding of MeCP2 to CpG island-2, -3, -4, and -5. Normal rabbit IgG (control) and anti-MeCP2 antibody (MeCP2) were used to immunoprecipitate the genomic region of each CpG island. Size markers (100 bp ladder) are shown at the left.

P28 to expression at P14 in the *Mecp2*-deficient mice was significantly higher than in wild-type mice (wild-type mice: 2.02 ± 0.14 fold; *Mecp2*-deficient mice: 2.70 ± 0.21 fold, $p = 0.0098$, $n = 4$). These results suggested that MeCP2 is involved in regulating expression of the novel *Shank3c* transcript in intron 10.

## Discussion

In this study, we identified two novel splicing *Shank3* transcript variants whose transcriptional initiation sites are located in intron 10. Sequence analysis revealed that the major *Shank3* transcript variant consisted of part of intron 10 and a completely spliced form from exon 11 to exon 22. We then demonstrated that the predicted translational start codon is located at position −77 in intron 10. Thus, this novel *Shank3* transcript probably produced the amino-terminus truncated SHANK3 isoform containing the Src homology 3 and following domains, including the post-synaptic density 95/discs large/zone occludens-1 domain, the homer-binding region, the cortactin-binding region, and SAM at its carboxyl-terminus. We investigated its expression profile in the developing mouse neocortex by performing a quantitative RT-PCR and immunoblot analysis. The transient decrease in its expression at P14 shown in Fig. 2 is unique. The result of the immunoblot analysis suggested that the lower expression of the transcript at P14 might be responsible for the reduction in protein after P14, especially at P21 (Fig. 6). Interestingly, the DNA methylation rate in CpG island-2, which is located near the transcriptional initiation site of the novel *Shank3* transcript and its promoter, increased at P14 and MeCP2 bound the CpG island-2 region. On the basis of the role of MeCP2 in transcriptional regulator via binding to the methylated DNA (Chahrour *et al.* 2008; Hite *et al.* 2009), we hypothesized that expression of the novel *Shank3* transcript is regulated by MeCP2. To test our hypothesis, we investigated expression of the novel *Shank3* transcript in *Mecp2*-deficient mice. Since a previous study showed that the synapses of *Mecp2*-deficient mice were less mature than in wild-type mice (Fukuda *et al.* 2005), we initially examined the expression of PSD-95 at P7, P14, and P28, and the results showed lower expression in *Mecp2*-deficient mice after P14, as expected. The level of expression of the full-length *Shank3* (*Shank3a*) transcript was also lower in *Mecp2*-deficient mice than in wild-type mice, especially at P14 and P28, when synapses were immature. We also demonstrated a difference between the expression profiles of the novel *Shank3* transcript (*Shank3c*) in wild-type mice and *Mecp2*-deficient mice. The rate of increase in expression level of the novel *Shank3* transcript from P14 to P28 was significantly higher than in the wild-type mice. These findings suggest that *Shank3* may be one of the target genes of MeCP2 and that the unbalanced expression of *Shank3* transcripts is implicated in the etiology of the synaptic abnormality caused by the dysfunction of MeCP2 in Rett syndrome.

Cumulative evidence has shown that several SHANK3 isoforms in human and rodent brains are produced as a result of complex transcriptional regulation by multiple intragenic promoters and extensive alternative splicing processes, and six different SHANK3 isoforms (SHANK3a-f) have been demonstrated thus far (Wang *et al.* 2011; Jiang and Ehlers 2013). Judging from gene and protein structures, the novel *Shank3* transcripts identified in this study likely code the SHANK3c isoforms reported in recent papers (Wang *et al.* 2011; Jiang and Ehlers 2013). Both papers reported demonstrating that the *Shank3c* transcript is expressed under promoter 3 located in intron 10, but the reports regarding the transcriptional initiation site of the *Shank3c* transcript are confusing. In Wang's paper, the transcriptional initiation site of the *Shank3*c transcript is reported to be located in intron 11, and two transcripts (*Shank3c-1* and *Shank3c-2*; GenBank: HQ405757 and HQ405758) are shown originating at the same initiation site. Since the transcriptional initiation site of *Shank3c-1* and *Shank3c-2* is different from that of the 22t *Shank3* transcript expressed in intron 11, they are not identical to the 22t *Shank3* transcript (Maunakea *et al.* 2010). On the other hand, the transcriptional initiation site reported in the review article by Jiang and Ehlers is located in intron 10. Based on all the above taken together, since the novel *Shank3* transcript identified in this study is one of the *Shank3c* transcripts, we designated it *Shank3c-3* (GenBank: AB841411). The other variant identified in the present study, designated *Shank3c-4* (GenBank: AB841412), lacks the sequences coded by exon 21, which results in production of the carboxyl-terminus truncated SHANK3 lacking the homer-binding region, the cortactin-binding region and the SAM. We identified a difference in the distribution of

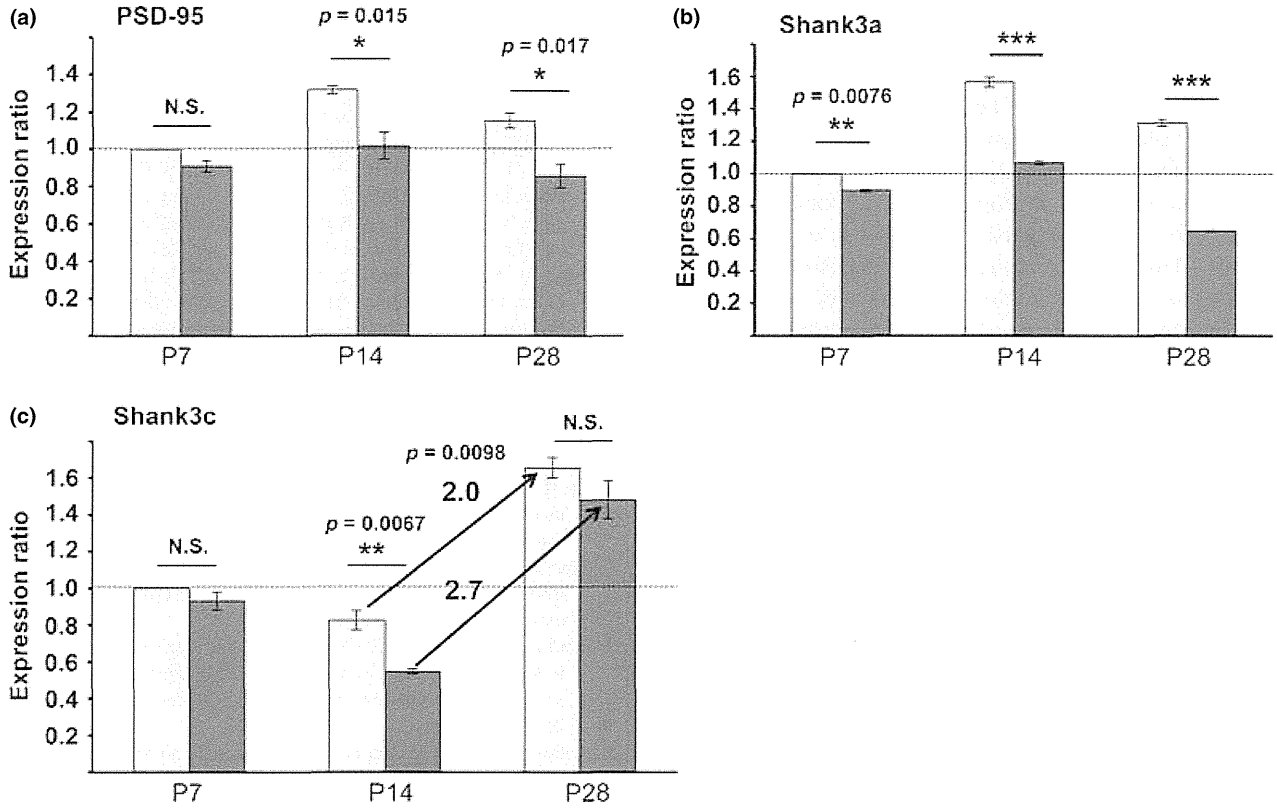


**Fig. 9** Analysis of expression of the novel *Shank3* transcript in *Mecp2*-deficient mice by a real-time PCR. Neocortical samples were prepared at P7, P14, and P28, and real-time PCR was performed to investigate the expression of PSD-95 (a), the major form of *Shank3* amplified by the 5UTR-F and CpGP-R primer pair (Shank3a) (b), and the novel *Shank3* transcript amplified by the In10-F and Ex14-R primer pair (Shank3c) (c). A quantitative analysis was performed by the delta-delta Ct method with glyceraldehyde-3-phosphate dehydrogenase as an internal control. Ratios were calculated by dividing the value at each stage by the value at P7 in wild-type mice. Light gray columns represent the wild-type mice and dark gray columns represent the *Mecp2*-deficient mice. The real-time PCR was independently performed four times with triplet samples from each individual. More than three pups at each stage were obtained from more than two families. $*p < 0.05$, $**p < 0.01$, $***p < 0.001$, N.S. = not significant.

the isoform containing the entire carboxyl-terminus sequence in the primary cultured neurons and the distribution of the isoform lacking the sequences coded by exon 21. As shown in Figure 7, SHANK3c-3 was predominantly expressed in the dendritic spines, whereas SHANK3c-4 was diffusely expressed in both the dendrites and axons. These findings were highly consistent with the results of a previous study that showed that the carboxyl-terminus truncated SHANK3 lacking the cortactin-binding region and the SAM were not targeted to synapses and were diffusely distributed throughout the neurons (Boeckers *et al.* 2005). Interestingly, the *Shank3b* transcript (GenBank: AJ245904) is known to be one of the alternative splicing variants of *Shank3* (Jiang and Ehlers 2013). Since the predicted translational start site is located in intron 2, and the sequence coded by exon 21 is absent in the *Shank3b* transcript, the product of the *Shank3b* transcript contains ankyrin repeats but no homer-binding region, cortactin-binding region, and SAM, however, the expression profile of the *Shank3b* transcript has not been elucidated. On the other hand, a recent genetic study of ASD patients identified two siblings who were heterozygous for a guanine residue insertion in exon 21 that resulted in a frameshift and a carboxyl-terminus truncated SHANK3 protein lacking the homer-binding region and following regions (SHANK3ΔC) (Durand *et al.* 2007). Thus, the presence of the carboxyl-terminus truncated SHANK3 isoforms, including the *Shank3b* transcript and the splicing variant of the novel *Shank3* transcript expressed from intron 10 (*Shank3c-4*), may be essential in the brain, but regulation of their expression is critical to organize synaptic function, and abnormal expression of carboxyl-terminus truncated SHANK3 may cause brain dysfunction, including ASD.

Several lines of *Shank3* mutant mice have been generated recently. Targeting of exons 4–9 (Bozdagi *et al.* 2010; Wang *et al.* 2011; Yang *et al.* 2012) and exons 4–7 (Peça *et al.* 2011) resulted in the disruption of full-length SHANK3 (SHANK3a) and SHANK3b, but SHANK3c-f remained. The targeting of exons 13–16 (Peça *et al.* 2011), on the

other hand, led to the elimination of SHANK3c-d in addition to SHANK3a and SHANK3b. *Shank3* mutant mice exhibit a variety of behavioral deficits, including compulsive and repetitive behavior, enhanced anxiety, and impaired social interaction, all of which resemble the cardinal features of ASD. Furthermore, Schmeisser and coworkers produced a *Shank3* mutant mouse strain in which exon 11 was targeted (Schmeisser *et al.* 2012). Their *Shank3* mutant mouse can produce SHANK3d-f but not SHANK3a-c, but the results of a behavioral analysis have not yet been reported. As a means of identifying the brain region and neural cells that are related to the behavioral deficits caused by the disruption of SHANK3, we used the Cre/LoxP system to develop a conditional knockout mouse in which the genomic region from intron10 to intron 12 is targeted. The ability to spatiotemporally disrupt SHANK3a-c isoforms in a Cre-recombinase-expression-dependent manner makes it possible to investigate the function of the SHANK3 isoforms in individual brain regions. Our next study is designed to reveal the genetic and protein structures of SHANK3 isoforms and to clarify their contributions in the neuronal network that causes autistic behaviors.

## Acknowledgements

This study was supported by grants from the Ministry of Health, Labour and Welfare of Japan (SU), the Ministry of Education, Culture, Sports, and Science and Technology of Japan (CW), and The Japan Foundation for Pediatric Research (SU). The authors have no conflicts of interest to declare.

## Supporting information

Additional supporting information may be found in the online version of this article at the publisher's web-site:

**Figure S1.** Schematic diagram of the construction of EGFP expression vector pGL3-In10-EGFP by a two-step PCR method.

**Figure S2.** Schematic diagram of the construction of the myc-tagged SHANK3 isoform expression vectors, pCAGGS-myc-Shank3c-3 and pCAGGS-myc-Shank3c-4.

**Data S1.** Plasmid construction.

## References

Amir R. E., Van den Veyver I. B., Wan M., Tran C. Q., Francke U. and Zoghbi H. Y. (1999) Rett syndrome is caused by mutations in X-linked *MECP2*, encoding methyl-CpG-binding protein 2. *Nat. Genet.* **23**, 185–188.

Beri S., Tonna N., Menozzi G., Bonaglia M. C., Sala C. and Giorda R. (2007) DNA methylation regulates tissue-specific expression of Shank3. *J. Neurochem.* **101**, 1380–1391.

Boeckers T. M., Segger-Junius M., Iglauer P., Bockmann J., Gundelfinger E. D., Kreutz M. R., Richter D., Kindler S. and Kreienkamp H.-J. (2004) Differential expression and dendritic transcript localization of Shank family members: identification of a dendritic targeting element in 3' untranslated region of Shank1 mRNA. *Mol. Cell. Neurosci.* **26**, 182–190.

Boeckers T. M., Liedtke T., Spilker C., Dresbach T., Bockmann J., Kreutz M. R. and Gundelfinger E. D. (2005) C-terminal synaptic targeting elements for postsynaptic density proteins ProSAP1/Shank2 and ProSAP2/Shank3. *J. Neurochem.* **92**, 519–524.

Bonaglia M. C., Giorda R., Borgatti R., Felisari G., Gagliardi C., Selicorni A. and Zuffardi O. (2001) Disruption of the ProSAP2 gene in a t(12;22)(q24.1;q13.3) is associated with the 22q13.3 deletion syndrome. *Am. J. Hum. Genet.* **69**, 261–268.

Bozdagi O., Sakurai T., Papapetrou D. *et al.* (2010) Haploinsufficiency of the autism-associated *Shank3* gene leads to deficits in synaptic function, social interaction, and social communication. *Mol. Autism* **1**, 15.

Chahrour M., Jung S. Y., Shaw C., Zhou X., Wong S. T. C., Qin J. and Zoghbi H. Y. (2008) MeCP2, a key contributor to neurological disease, activates and represses transcription. *Science* **320**, 1224–1229.

Ching T.-T., Maunakea A. K., Jun P. *et al.* (2005) Epigenome analyses using BAC microarrays identify evolutionary conservation of tissue-specific methylation of SHANK3. *Nat. Genet.* **37**, 645–651.

Chomczynski P. and Sacchi N. (1987) single-step method of RNA isolation by acid guanidinium thiocyanate-phenol-chloroform extraction. *Anal. Biochem.* **162**, 156–159.

Durand C. M., Betancur C., Boeckers T. M. *et al.* (2007) Mutations in the gene encoding the synaptic scaffolding protein SHANK3 are associated with autism spectrum disorders. *Nat. Genet.* **39**, 25–27.

Ermolinsky B., Pacheco Otalora L. F., Arshadmansab M. F., Zarei M. M. and Garrido-Sanabria E. R. (2008) Differential changes in mGlu2 and mGlu3 gene expression following pilocarpine-induced status epilepticus: a comparative real-time PCR analysis. *Brain Res.* **1226**, 173–180.

Fukuda T., Itoh M., Ichikawa T., Eashiyama K. and Goto Y. (2005) Delayed maturation of neuronal architecture and synaptogenesis in cerebral cortex of *Mecp2*-deficient mice. *J. Neuropathol. Exp. Neurol.* **64**, 537–544.

Gauthier J., Spiegelman D., Piton A. *et al.* (2009) Novel de novo SHANK3 mutation in autistic patients. *Am. J. Med. Genet. Part B.* **150B**, 421–424.

Guy J., Hendrich B., Holmes M., Martin J. E. and Bird A. (2001) A mouse Mecp2-null mutation causes neurological symptoms that mimic Rett syndrome. *Nat. Genet.* **27**, 322–326.

Hirasawa T., Wada H., Kohsaka S. and Uchino S. (2003) Inhibition of NMDA receptors induces delayed neuronal maturation and sustained proliferation of progenitor cells during neocortical development. *J. Neurosci. Res.* **74**, 676–687.

Hite K. C., Adams V. H. and Hansen J. C. (2009) Recent advances in MeCP2 structure and function. *Biochem. Cell Biol.* **87**, 219–227.

Jiang Y.-H. and Ehlers M. D. (2013) Modeling autism by *SHANK* gene mutations in mice. *Neuron* **78**, 8–27.

Lam C.-W. (2000) Spectrum of mutations in the *MECP2* gene in patients with infantile autism and Rett syndrome. *J. Med. Genet.* **37**, E14.

Lim S., Naisbitt S., Yoon J., Hwang J.-I., Suh P.-G., Sheng M. and Kim E. (1999) Characterization of the Shank family of synaptic proteins. Multiple genes, alternative splicing, and differential expression in brain and development. *J. Biol. Chem.* **274**, 29510–29518.

Maunakea A. K., Nagarajan R. P., Bilenky M. *et al.* (2010) Conserved role of intragenic DNA methylation in regulating alternative promoter. *Nature* **466**, 253–257.

Moessner R., Marshall C. R., Sutcliffe J. S. *et al.* (2007) Contribution of *SHANK3* mutations to autism spectrum disorder. *Am. J. Hum. Genet.* **81**, 1289–1297.

Naisbitt S., Kim E., Tu J. C., Xiao B., Sala C., Valtsvhanoff J., Weinberg R. J., Worley P. E. and Sheng M. (1999) Shank3, a novel family of postsynaptic density proteins that binds to the NMDA receptor/PSD-95/GKAP complex and cortactin. *Neuron* **23**, 569–582.

Peça J., Feliciano C., Ting J. T., Wang W., Wells M. F., Venkatraman T. N., Lascola C. D., Fu Z. and Feng G. (2011) *Shank3* mutant mice display autistic-like behaviours and striatal dysfunction. *Nature* **472**, 437–442.

Schmeisser M. J., Ey E., Wegener S. *et al.* (2012) Autistic-like behaviours and hyperactivity in mice lacking ProSAP1/Shank2. *Nature* **486**, 261–265.

Sheng M. and Kim E. (2000) The Shank family of scaffold proteins. *J. Cell Sci.* **113**, 1851–1856.

Uchino S., Wada H., Honda S., Nakamura Y., Ondo Y., Uchiyama T., Tsutsumi M., Suzuki E., Hirasawa T. and Kohsaka S. (2006) Direct interaction of post-synaptic density-95/Dlg/ZO-1 domain-containing synaptic molecule Shank3 with GluR1 α-amino-3-hydroxy-5-methyl-4-isoxazole propionic acid receptor. *J. Neurochem.* **97**, 1203–1214.

Waga C., Okamoto N., Ondo Y., Fukumura-Kato R., Goto Y., Kohsaka S. and Uchino S. (2011) Novel variants of the *SHANK3* gene in Japanese autistic patients with severe delayed speech development. *Psychiat. Genet.* **21**, 208–211.

Wang X., McCoy P. A., Rodriguiz R. M. *et al.* (2011) Synaptic dysfunction and abnormal behaviors in mice lacking major isoforms of *Shank3*. *Hum. Mol. Genet.* **20**, 3093–3108.

Yamada Y., Watanabe H., Miura F., Soejima H., Uchiyama M., Iwasaka T., Mukai T., Sakaki Y. and Ito T. (2004) A comprehensive analysis of allelic methylation status of CpG islands on human chromosome 21q. *Genome Res.* **14**, 247–266.

Yang M., Bozdagi O., Scattoni M. L. *et al.* (2012) Reduced excitatory neurotransmission and mild autism-relevant phenotypes in adolescent *Shank3* null mutant mice. *J. Neurosci.* **32**, 6525–6541.

 

ELSEVIER

Brain & Development 36 (2014) 794–800

BRAIN & DEVELOPMENT
Official Journal of the Japanese Society of Child Neurology

www.elsevier.com/locate/braindev

Original article

# Relation between circulating levels of GH, IGF-1, ghrelin and somatic growth in Rett syndrome

Munetsugu Hara [a], Yoshihiro Nishi [b], Yushiro Yamashita [c], Rumiko Hirata [c], Satoru Takahashi [d], Shin-ichiro Nagamitsu [c], Hiroshi Hosoda [e], Kenji Kangawa [e], Masayasu Kojima [f], Toyojiro Matsuishi [c,*]

[a] *Department of Neonatology, Medical Center for Maternal and Child Health, St. Mary's Hospital, Kurume, Fukuoka 830-8543, Japan*
[b] *Department of Physiology, Kurume University School of Medicine, 67 Asahi-machi, Kurume, Fukuoka 830-0011, Japan*
[c] *Department of Pediatrics and Child Health, Kurume University School of Medicine, 67 Asahi-machi, Kurume, Fukuoka 830-0011, Japan*
[d] *Department of Pediatrics, Asahikawa Medical University, Asahikawa, Hokkaido 078-8510, Japan*
[e] *Department of Biochemistry, National Cardiovascular Center Research Institute, Suita, Osaka 565-8565, Japan*
[f] *Institute of Life Science, Kurume University, Hyakunenkohen, Kurume, Fukuoka 839-0864, Japan*

Received 18 January 2013; received in revised form 6 November 2013; accepted 18 November 2013

**Abstract**

*Background:* Most cases of Rett syndrome (RTT) are caused by mutations in *methyl CpG binding protein 2* (*MECP2*), and individuals with RTT have somatic growth failure, growth arrest of brain, epilepsy, and intellectual disability (ID). Ghrelin is a peptide hormone which stimulates growth hormone (GH) secretion from the pituitary gland. Ghrelin and GH regulate insulin-like growth factor-1 (IGF-1) synthesis, and this GH/IGF-1 axis is an endocrine axis involved in energy and sleep homeostasis and plays crucial roles in somatic and brain growth. This study aimed to determine whether circulating ghrelin, GH and IGF-1 reflect somatic and brain growth in RTT patients. *Methods:* We examined anthropometric data and circulating ghrelin, GH, and IGF-1 in 22 female RTT patients with epilepsy and ID (RTT-Ep/ID) and 14 age-matched females with epilepsy and ID (non-RTT-Ep/ID). *Results:* Body mass index (BMI) and height/length were significantly lower in RTT-Ep/ID than in non-RTT-Ep/ID in patients less than 20 years old. Plasma ghrelin in RTT-Ep/ID patients showed a significant inverse correlation with weight but had no significant correlations with BMI or height. Head circumference in both groups showed a significant positive correlation with circulating ghrelin and a significant negative correlation with circulating IGF-1. The ratio of octanoyl-ghrelin to total-ghrelin (O/T-ratio) is used as an indicator to estimate the biological activity of ghrelin. Among pre-adolescents, O/T-ratios were significantly higher in the RTT-Ep/ID group than in the non-RTT-Ep/ID group ($P < 0.05$). *Conclusions:* Timing of growth-spurts differed between the RTT-Ep/ID and non-RTT-Ep/ID groups, possibly due to a common (but yet unknown) mechanism of growth failure. Ghrelin/GH/IGF-1 axis function was aberrant in both the RTT-Ep/ID and non-RTT-Ep/ID groups. The initial clinical course of Rett syndrome affects the development of the sleep–wake cycle and locomotion in early infancy, both of which may be based on the dysfunction of the aminergic neurons modulated by ghrelin/GH/IGF-1 axis. Further study with a larger sample size should help clarify the precise mechanisms controlling the somatic growth and hormonal features in Rett syndrome.


*Keywords:* Rett syndrome; MECP2; Intellectual disability; Growth; Ghrelin; GH; IGF-1

## 1. Introduction

Rett syndrome (RTT; MIM 312750) is an X-linked neurodevelopmental disorder caused by mutations in

* Corresponding author. Tel.: +81 942 31 7565; fax: +81 942 38 1792.
*E-mail address:* tmatsu@med.kurume-u.ac.jp (T. Matsuishi).

0387-7604/$ - see front matter © 2013 The Japanese Society of Child Neurology. Published by Elsevier B.V. All rights reserved.
http://dx.doi.org/10.1016/j.braindev.2013.11.007

*methyl CpG binding protein 2* (*MECP2*) [1]. RTT is characterized by somatic growth failure following the deceleration of head growth, intellectual disability, erratic and purposeless rhythmic movement and sleep disruption [2,3]. Somatic growth failure is a major aspect of the developmental arrest. In a population-based cohort, the mean weight, height, and body mass index *Z* scores in subjects with RTT were below those of their age group in the general population and decreased steadily with age. Moreover, growth failure occurs less frequently in girls and women with better development and less morbidity typically associated with RTT, and in those with late truncation mutations or C terminal mutations of the *MECP2* gene [4–6]. The growth hormone (GH)/insulin-like growth factor-1 (IGF-1) axis has essential roles in somatic growth. Ghrelin is a peptide hormone involved in the GH/IGF-1 axis. Ghrelin secreted during fasting promotes the secretion of GH through the GH secretagogue receptor (GHS-R) and this in turn promotes the synthesis and secretion of IGF-1 [7,8]. The Ghrelin/GH/IGF-1 axis is an endocrine axis involved in energy and sleep homeostasis [9]. Plasma concentration of ghrelin is negatively regulated by circulating IGF-1 [8]. GH regulates somatic growth and development directly through the activation of GH receptors and indirectly through IGF-1 [10,11]. IGF-1 mediates tissue formation and remodeling, bone growth, postnatal growth and muscle metabolism [11,12]. IGF-1 is widely expressed in the central nervous system (CNS) [13], where it regulates neuronal and glial cell proliferation, and strongly promotes neuronal cell survival and synaptic maturation [13,14]. In genetically modified mice, postnatal overexpression of IGF-1 contributed to brain overgrowth characterized by an increase in the number of neurons and oligodendrocytes [13]. In contrast, ablation of IGF-1 and IGF-1 receptor (IGF-1R) expression resulted in growth retardation not only of body but also of brain [14]. In the CNS, ghrelin is synthesized mainly at the hypothalamus [15], whereas its receptor, GHS-R type 1a, is broadly distributed within the CNS [11]. Ghrelin promotes cell proliferation in both the embryonic and adult nervous systems [11] and stimulates the proliferation of neuronal precursor cells through GHS-R [16]. Moreover, ghrelin modifies the sleep–wake (S–W) rhythm by increasing wakefulness and decreasing the duration of REM sleep periods via GHS-R in the hypothalamus and pituitary gland [17]. S–W rhythm is related to GH ultradian rhythmicity in humans [18]. Maximal GH release occurred within minutes of the sleep onset of stage 3 or 4 sleep [17]. Ghrelin secretion is pulsatile and displays an ultradian rhythmicity. The number of peaks and the interval between peaks of ghrelin are similar to those observed for GH secretion, whereas peak amplitudes are much more important for GH [17]. Consequently, ghrelin and the GH/IGF-1 axis play crucial roles not only in somatic growth and but also in CNS development. In our previous work, plasma ghrelin levels were high during infancy in RTT patients, then decreased whereas plasma ghrelin levels increased at puberty in healthy controls [19]; however, we did not examine the relationship between somatic growth disturbances and circulating levels of GH and IGF-1, in RTT. Moreover, we did not compare plasma ghrelin levels between patients with RTT and patients with epilepsy and intellectual disability (Ep/ID), although there is a high incidence of Ep/ID in RTT patients [19]. Therefore, in the present study we compared the circulating ghrelin, GH and IGF-1 concentrations and anthropometric data, i.e., weight, height, body mass index (BMI), and occipito-frontal head circumference (OFC), in RTT and non-RTT patients with Ep/ID.

## 2. Methods

Clinical diagnosis of RTT was confirmed in 22 female patients according to the recently proposed RTT Diagnostic Criteria [2]. The age of our RTT-Ep/ID patients ranged from 4.0 to 37.5 years old. RTT patients manifested sleep disruptions (18/22) and periodic breathing (14/22). Plasma concentrations of ghrelin, GH and IGF-1 were measured in the RTT-Ep/ID patients and in 14 age-matched female patients with epilepsy and intellectual disability (Ep/ID; age range 3.3–23.9 years old). *MECP2* mutations were confirmed in all 22 RTT-Ep/ID patients by *MECP2* gene analysis. All had a developmental quotient (DQ) or intelligence quotient (IQ) below 20. Of the 14 patients with non-RTT-Ep/ID, seven had profound retardation (IQ < 20), one had severe ID (IQ = 20–34), two had moderate ID (IQ = 35–49), three had mild ID (IQ = 50–69), and one had an IQ below 70 (precise score unknown). None of the participants received autonomic nerve regulators or had undergone gastrostomy. We also collected the participants' clinical data (including age for developmental comparisons): 0–10 yr-olds [RTT-Ep/ID, $n = 7$; non-RTT-Ep/ID, $n = 6$], 10–20 yr-olds [RTT-Ep/ID, $n = 10$; non-RTT-Ep/ID, $n = 6$], and over-20-year-olds [RTT-Ep/ID, $n = 5$; non-RTT-Ep/ID, $n = 2$]), weight, height, BMI and occipito-frontal head circumference (OFC). These data were converted into standard deviation (*Z* score) values based on the U.S. National Center for Health Statistics/World Health Organization references [20]. Written informed consent was obtained from a parent for each patient. The study protocol was approved by the Ethics Committee of the Kurume University School of Medicine.

## 3. Measurement of plasma ghrelin levels

The extraction of plasma ghrelin from blood was performed by a method described previously [21,22]. The separated plasma samples were stored at −80 °C within

5 min to prevent degradation of rapidly regulated proteins. The plasma samples were semi-purified with a Sep-Pak C18 cartridge before the ghrelin radioimmunoassay (RIA). Two ghrelin-specific RIAs were used; one, named N-RIA, recognizes the N-terminal portion of octanoyl-modified active ghrelin, and the other, named C-RIA, recognizes the C-terminal portion of ghrelin irrespective of its octanoyl modification. The plasma level of octanoyl-ghrelin, which is post-transnationally octanoylated at Ser3, was measured by N-RIA [21,23]. The plasma level of total ghrelin, i.e. the sum of the non-octanoyl and octanoyl ghrelin levels, was measured by C-RIA.

### *3.1. Measurement of serum growth hormone (GH) and insulin-like growth factor-1 (IGF-1) levels*

Serum concentrations of GH and IGF-1 were measured in duplicate by immunoradiometric assays according to the manufacturer's protocol (Active Growth Hormone IRMA DSL-1900 and Active Non-Extraction IGF-1 IRMA DSL-2800, respectively, Diagnostics System Laboratories, Webster, TX) or a radioimmunoassay kit (SRL, Tokyo). Each assay was calibrated with manufacturer-supplied standards.

### *3.2. Statistical analysis*

The concentrations of plasma total- and octanoyl-ghrelin and serum GH and IGF-1 were compared between the two subject groups by *t*-tests, and Pearson's correlation coefficients were used to measure monotonic associations between variables. The data are summarized as mean ± standard deviations (s.d.). *P*-values $\leqslant 0.05$ were considered significant.

## 4. Results

The mean values of BMI-for-age and height/length-for-age *Z* scores in RTT-Ep/ID patients were significantly lower than those of non-RTT-Ep/ID patients (Table 1). Conversely, the octanoyl-/total-ghrelin ratios in RTT-Ep/ID patients were significantly higher than those of non-RTT-Ep/ID patients. The developmental data (Table 2) show that the serum GH concentrations in RTT-Ep/ID patients were significantly lower than those of non-RTT-Ep/ID patients between the ages of 0 and 10 years. The means of the height/length-for-age *Z* score of RTT-Ep/ID patients between the ages of 0 and 20 years were significantly lower than those of non-RTT-Ep/ID patients within the same age range. Over 20 years old, the mean of the height/length-for-age *Z* score of RTT-Ep/ID patients was similar to that of non-RTT-Ep/ID patients. On the other hand, the octanoyl-/total-ghrelin ratios of RTT-Ep/ID patients between the ages of 0 and 20 years were significantly higher than those of non-RTT-Ep/ID patients within the same age range. There were no significant differences in plasma concentrations of total- and octanoyl-ghrelin or serum concentrations of GH and IGF-1 between the two groups. Plasma total- and octanoyl-ghrelin concentrations, and the serum GH and IGF-1 concentrations showed no significant correlation with height/length-for-age *Z* score in either group. As shown in

Table 1
Characteristics of the RTT-Ep/ID and non-RTT-Ep/ID patients.

| Characteristics | RTT-Ep/ID ($n = 22$) | | Non-RTT-Ep/ID ($n = 14$) | | *p* |
|---|---|---|---|---|---|
| | Mean ± s.d | Range | Mean ± s.d | Range | |
| Age (years) | 16.44 ± 8.56 | 4.00–37.50 | 11.77 ± 6.23 | 3.25–23.92 | 0.09 |
| Weight (kg) | 28.90 ± 12.44 | 11.60–54.00 | 31.53 ± 13.82 | 11.40–61.00 | 0.56 |
| Weight-for-age (*Z* score) | −0.86 ± 2.17 | −4.35–2.52 | 0.35 ± 1.56 | −2.22–3.12 | 0.06 |
| BMI (kg/m$^2$) | 15.57 ± 3.64 | 9.70–22.80 | 17.41 ± 3.69 | 12.41–25.65 | 0.15 |
| BMI-for-age (*Z* score) | −2.18 ± 2.17 | −7.91–0.50 | −0.47 ± 1.73 | −3.02–3.16 | 0.02* |
| Height/length (cm) | 133.01 ± 19.59 | 88.10–156.5 | 131.41 ± 23.46 | 91.30–169.30 | 0.83 |
| Height/length-for-age (*Z* score) | −2.68 ± 0.85 | −3.99–−1.02 | −1.30 ± 1.01 | −3.47–0.94 | 0.00** |
| OFC (cm) | 50.64 ± 2.48 | 46.50–54.30 | 50.77 ± 2.46 | 46.80–54.30 | 0.88 |
| OFC-for-age (*Z* score) | 0.52 ± 1.73 | −2.41–3.08 | 0.70 ± 1.57 | −2.19–3.08 | 0.76 |
| Total ghrelin (fmol/ml) | 127.80 ± 87.62 | 39.72–442.72 | 164.77 ± 113.27 | 21.92–454.75 | 0.28 |
| Octanoyl ghrelin (fmol/ml) | 17.76 ± 8.80 | 2.75–32.13 | 12.56 ± 9.47 | 2.00–30.84 | 0.10 |
| Octanoyl-/total-ghrelin ratio | 16.26 ± 6.64 | 5.91–29.31 | 7.68 ± 3.78 | 3.45–18.14 | 0.00** |
| GH (ng/ml) | 1.62 ± 2.60 | 0.05–11.50 | 2.10 ± 1.91 | 0.15–5.75 | 0.56 |
| IGF-1 (ng/ml) | 168.25 ± 96.12 | 60.31–375.00 | 201.57 ± 92.69 | 47.00–350.00 | 0.31 |
| IGF-1/GH ratio | 618.13 ± 1194.27 | 30.43–5540.00 | 367.79 ± 601.71 | 15.06–2333.33 | 0.47 |

The data are means ± s.d. Ep: epilepsy; ID: intellectual disability; RTT: Rett syndrome; OFC: occipito-frontal head circumference. The means of BMI-for-age *Z* score, height/length-for-age *Z* score, and octanoyl-/total ghrelin ratio in the RTT-Ep/ID group were significantly different compared to those of the non-RTT-Ep/ID group.
* $p < 0.05$ (*t*-test).
** $p < 0.01$ (*t*-test).

Table 2
Developmental characteristics of the RTT-Ep/ID and non-RTT-Ep/ID patients.

| Characteristics | 0–10 (years) | | p | 10–20 (years) | | p | >20 (years) | | p |
|---|---|---|---|---|---|---|---|---|---|
| | RTT-Ep/ID ($n = 7$) | Non-RTT-Ep/ID ($n = 6$) | | RTT-Ep/ID ($n = 10$) | Non-RTT-Ep/ID ($n = 6$) | | RTT-Ep/ID ($n = 5$) | Non-RTT-Ep/ID ($n = 2$) | |
| | Mean ± s.d. | Mean ± s.d. | | Mean ± s.d | Mean ± s.d | | Mean ± s.d. | Mean ± s.d. | |
| Weight-for-age ($Z$ score) | −3.14 ± 0.78 | −0.28 ± 1.53 | 0.00** | −0.42 ± 1.78 | 0.16 ± 1.02 | 0.48 | 1.44 ± 0.78 | 2.78 ± 0.48 | 0.64 |
| BMI-for-age ($Z$ score) | −1.74 ± 1.11 | 0.28 ± 2.17 | 0.05 | −3.02 ± 2.87 | −1.39 ± 1.13 | 0.21 | −1.09 ± 1.11 | 0.05 ± 0.00 | 0.15 |
| Height/length-for-age ($Z$ score) | −2.84 ± 0.77 | −1.24 ± 0.78 | 0.00** | −2.96 ± 0.65 | −1.73 ± 0.89 | 0.01* | −1.88 ± 0.77 | −0.17 ± 1.57 | 0.13 |
| OFC-for-age ($Z$ score) | −1.20 ± 0.98 | −0.43 ± 1.34 | 0.26 | 1.06 ± 1.55 | 1.26 ± 1.16 | 0.79 | 1.87 ± 0.98 | 2.41 ± 0.94 | 0.50 |
| Total ghrelin (fmol/ml) | 208.34 ± 107.84 | 226.22 ± 157.49 | 0.81 | 91.56 ± 45.68 | 123.50 ± 18.27 | 0.13 | 87.51 ± 107.84 | 104.25 ± 30.25 | 0.61 |
| Octanoyl ghrelin (fmol/ml) | 26.85 ± 4.28 | 17.16 ± 11.33 | 0.09 | 12.15 ± 6.32 | 7.87 ± 3.62 | 0.16 | 16.27 ± 4.28 | 12.83 ± 14.09 | 0.68 |
| Octanoyl-/total-ghrelin ratio | 14.91 ± 5.63 | 7.98 ± 1.54 | 0.01* | 15.84 ± 7.80 | 6.36 ± 2.67 | 0.01* | 19.00 ± 5.63 | 10.80 ± 10.39 | 0.22 |
| GH (ng/ml) | 0.93 ± 0.96 | 3.05 ± 1.90 | 0.03* | 2.32 ± 3.65 | 1.62 ± 1.91 | 0.67 | 1.16 ± 0.96 | 0.68 ± 0.52 | 0.65 |
| IGF-1 (ng/ml) | 127.11 ± 43.34 | 154.00 ± 103.39 | 0.55 | 183.38 ± 119.92 | 250.00 ± 76.60 | 0.25 | 195.60 ± 43.34 | 199.00 ± 35.36 | 0.96 |
| IGF-1/GH ratio | 302.77 ± 232.00 | 418.65 ± 938.17 | 0.76 | 480.89 ± 644.60 | 310.07 ± 204.78 | 0.54 | 1334.12 ± 2368.34 | 388.34 ± 244.59 | 0.62 |

The data are means ± s.d. The RTT-Ep/ID and non-RTT-Ep/ID groups were divided into the following age groups: 0–10 years old, 10–20 years old, and over 20 years old. The means of the weight-for-age $Z$ score, height/length-for-age $Z$ score, octanoyl-/total ghrelin ratio and the serum GH concentrations in the 0–10-years-old group with RTT were significantly different compared to those of the non-RTT-Ep/ID group in the same age range. The means of height/length-for-age $Z$ score and octanoyl-/total-ghrelin ratio in the 10–20-years-old group with RTT were significantly different compared to those of the non-RTT-Ep/ID group in the same age range. Abbreviations are explained in Table 1.
* $p < 0.05$ ($t$-test).
** $p < 0.01$ ($t$-test).

Table 3, plasma concentrations of total-ghrelin showed significantly negative correlations with age, weight, and OFC-for-age $Z$ score in both RTT-Ep/ID and non-RTT-Ep/ID patients, whereas the serum IGF-1 concentrations showed significantly positive correlations with weight, BMI-for-age and OFC-for-age $Z$ score in RTT-Ep/ID patients. The octanoyl-/total-ghrelin ratio showed a significantly positive correlation with OFC-for-age $Z$ score only in RTT-Ep/ID patients. No statistical analysis to present definite relationships between genotype and phenotype is possible because of the small sample size, as shown in Supplementary Table 1.

## 5. Discussion

It is well known that patients with RTT exhibit short statures compared to healthy individuals with normal somatic growth [2]. The mean growth of length, weight and head circumference in classic RTT fell below growth chart levels for the normative population and growth failure occurs less frequently in girls with RTT, who show better development, less morbidity typically associated with RTT, and late truncation mutations [5]. RTT patients with C-terminal deletions had the highest $Z$ scores for weight and BMI. Their BMI $Z$ scores were significantly higher when compared with all other mutations [4]. BMI, weight, and height $Z$ scores of RTT patients without enteral support did not identify statistically significant differences between any genotype groups. Isaacs et al. previously found that microcephaly was associated with lower weight-for-age $Z$ scores [24]. We previously reported that the mean values of weight, BMI, height/length and OFC-for-age $Z$ scores in RTT patients were lower than those of healthy controls, and that eating difficulties in RTT patients were significantly correlated with the plasma levels of total and octanoyl ghrelin [19]. Although eating difficulties may be caused by inadequate dietary intake, growth problems in Rett syndrome are also known to be related to the specific genotypes. Eating difficulties and growth failure in RTT patients with low levels of plasma ghrelin are also presumed to be caused by *MECP2* mutations. However we did not identify any statistically significant overall correlations between the $Z$ score and genetic profile because of small sample size.

In the present study, the time points for growth-spurts in RTT-Ep/ID children were delayed compared to those in non-RTT-Ep/ID children, whereas subsequently RTT-Ep/ID patients achieved growth in height equivalent to that of non-RTT-Ep/ID patients. Previously, we and others have reported that the values for occipito-frontal head circumference (OFC) in RTT-Ep/ID patients were significantly smaller than those in healthy controls [2,19]. However, in this study there was no significant difference in OFC values between the RTT-Ep/ID and non-RTT-Ep/ID groups. In most

Table 3
Correlation among anthropometric data and circulating ghrelin, GH and IGF-1 between the RTT-Ep/ID and non-RTT-Ep/ID patients.

| Characteristics | Total ghrelin | Octanoyl ghrelin | Octanoyl/total ghrelin ratio | IGF-1 | GH |
|---|---|---|---|---|---|
| *Non-RTT-Ep/ID (n = 14)* | | | | | |
| Age (years) | −0.62* | −0.49 | 0.05 | 0.36 | −0.43 |
| Weight-for-age (*Z* score) | −0.53* | −0.41 | 0.07 | 0.25 | −0.40 |
| BMI-for-age (*Z* score) | −0.08 | −0.07 | −0.00 | 0.04 | −0.24 |
| Height/Length-for-age (*Z* score) | 0.06 | 0.21 | 0.47 | 0.18 | 0.10 |
| OFC-for-age (*Z* score) | −0.60* | −0.50 | 0.05 | 0.52 | −0.67** |
| *RTT-Ep/ID (n = 22)* | | | | | |
| Age (years) | −0.44* | −0.37 | 0.21 | 0.25 | 0.01 |
| Weight-for-age (*Z* score) | −0.63* | −0.52* | 0.37 | 0.62** | 0.25 |
| BMI-for-age (*Z* score) | −0.10 | 0.09 | 0.32 | 0.65** | 0.24 |
| Height/Length-for-age (*Z* score) | −0.20 | 0.05 | 0.23 | −0.04 | −0.20 |
| OFC-for-age (*Z* score) | −0.72** | −0.55** | 0.47* | 0.58** | 0.22 |

Pearson's correlation coefficients were used to measure monotonic associations in the RTT-Ep/ID and non-RTT-Ep/ID groups. The plasma total-ghrelin concentrations showed a significantly negative correlation with age, weight-for-age *Z* score and OFC-for-age *Z* score in both the RTT and non-RTT-Ep/ID patients. The plasma octanoyl-ghrelin concentrations showed a significantly negative correlation with weight and OFC-for-age *Z* score only in the RTT-Ep/ID patients. The serum IGF-1 concentrations showed a significantly positive correlation with weight-for-age *Z* score, BMI-for-age *Z* score and OFC-for-age *Z* score only in the RTT-Ep/ID patients. Octanoyl-/total-ghrelin ratio showed a significantly positive correlation with OFC-for-age *Z* score only in the RTT-Ep/ID patients. The serum GH concentrations showed a significantly negative correlation with OFC-for-age *Z* score only in non-RTT-Ep/ID patients. Abbreviations are explained in Table 1.
* $p < 0.05$.
** $p < 0.01$.

children with postnatal-onset microcephaly, developmental outcome and somatic growth were markedly retarded [25]. In children with epilepsy, it was reported that onset of epileptic symptoms was preceded by a reduction in brain volume [26]. In disorders associated with ID, reductions in dendritic branch complexity and dendritic length, both of which bring about a reduction of brain volume, have been reported to be common pathological features [27]. These data supports the suggestion that the short stature and microcephaly of both groups may have been affected by epilepsy and intellectual disability during early infancy. However, the median age of onset of epilepsy in RTT is around 4 years [3]. This does not coincide with the timing of the deceleration of head growth. The deceleration of head growth and the characters of neuronal architecture may be partly determined by the genotype. On the other hand, the neurons and neuronal systems involved in the development of S–W rhythm and locomotion are affected in early infancy of RTT [28]. Segawa reported that this pathophysiology was based on the dysfunction of the aminergic neurons of the brainstem in early infancy. This causes autistic tendency and failure in synaptogenesis of the cortex and consequently causes microcephaly. Furthermore, this causes failure in restriction of atonia into REM stage. This induces dysfunction of the pedunculopontine nuclei (PPN) and consequently dysfunction of the dopamine neurons. This causes dysfunction of the supplementary motor area through the ascending pathway of the basal ganglia to the thalamus, consequently causes loss of purposeful hand use and induces the characteristic stereotyped hand movements. Ghrelin depolarizes PPN postsynaptically and dose-dependently via GHS-Rs [29]. The metabolic rate of girls with RTT was lower while sleeping, but not while awake, than in healthy controls [30]. Short stature, microcephaly and disorder of the circadian S–W cycle of RTT in early infancy may reflect the dysfunction of aminergic neurons modulated by the ghrelin/GH/IGF-1 axis.

In the present study, circulating levels of GH, IGF-1 and ghrelin in RTT-Ep/ID patients did not differ significantly from those in non-RTT-Ep/ID patients. Furthermore, the levels of circulating GH, IGF-1 or ghrelin were not significantly correlated with height in either group. On the other hand, our present study revealed a significant positive correlation between body weight and serum IGF-1 levels in RTT-Ep/ID patients. Within the RTT-Ep/ID group, we also found a significant inverse correlation between plasma octanoyl-ghrelin (active ghrelin) level and body weight. These findings are in line with those of previous reports demonstrating a positive correlation between serum IGF-1 level and body weight in a group of healthy children with normal growth [31]. Our findings are also supported by previous reports showing that the secretion of total ghrelin is negatively regulated by circulating IGF-1 through a negative-feedback loop [32]. IGF-1 ameliorates the RTT-like symptoms in a mouse model of the disease [33]. An Italian pilot study of RTT revealed that there are no risks associated with IGF1 administration [34].

In general, bone mineral deficits and bone-related disorders including fractures and scoliosis were common in RTT and deficits in bone mineral density were identified across a broad range of *MECP2* mutations [35]. In an

Australian Rett syndrome cohort study, the p.R168X and p.T158 M mutations predicted the low value of the areal bone mineral density and bone mineral content for all bone outcomes [36]. The activated ghrelin/GH/IGF-1 axis stimulates longitudinal bone growth and increases the body weights of growing children [37,38]. However, a study by Caffarelli et al., reported that plasma levels of ghrelin did not reflect longitudinal bone growth in female RTT patients within a growing period and both age and height were independent predictors of total body bone mineral density [39]. Similarly, the short stature of our RTT-Ep/ID patients (a consequence of insufficient longitudinal bone growth), could not be predicted by their circulating levels of ghrelin, GH or IGF-1. These findings in RTT may imply that ghrelin stimulation is insufficient to induce the required peak amplitudes of GH secretion [40], and this may be caused by the dysfunction of aminergic neurons from early infancy.

Octanoyl ghrelin is a major active form of ghrelin which is post-translationally modified with an octanoyl-group at its Ser3 residue [7]. In fact, the ratio of octanoyl-ghrelin to total-ghrelin (O/T-ratio) is used as an indicator to estimate the biological activity of ghrelin [41]. In our study, the O/T-ratio of patients less than 20 years old was significantly higher in the RTT-Ep/ID group than in the non-RTT-Ep/ID group. In addition, this O/T-ratio exhibited a significantly positive correlation with OFC-for-age $Z$ score only in RTT-Ep/ID patients. In comparison to non-RTT-Ep/ID patients, RTT-Ep/ID patients below the age of 20 had shorter height, smaller OFC, and a higher O/T-ratio. This unexpected finding may reflect alterations in respect of endocrine control by the ghrelin/GH/IGF-1 axis. On the other hand, these results coincide temporally with early development. These phenomena appear to occur independently and concurrently, as the result of epigenetic processes that temporally and spatially control gene activity during ontogenesis. Organ patterning and size are based on the spatiotemporal formation of morphogen gradients [42,43]. The *MECP2* gene determines cell fate, morphology and proliferation through posttranslational modifications [44]. In RTT, epigenetic regulation of gene expression involved in the morphogens linked to the growth of bone and brain and the enzymes mediating the modification of ghrelin may be improperly and irrelevantly influenced by *MECP2* mutation in early infancy.

This study has two major limitations. One is that we obtained results from single-time-point assays, and the other is the relatively small sample size of the groups (22 RTT-Ep/ID patients, 14 non-RTT-Ep/ID patients). The use of provocation tests (i.e. GHRH-loading test for GH) or measurement of the circadian profiles of ghrelin and other somatotropic hormones in a larger number of RTT-Ep/ID and non-RTT-Ep/ID patients, would allow us to evaluate the various functions of the ghrelin/GH/IGF-1 axis in more detail.

In conclusion, we found in this study a difference in the timing of growth-spurts between RTT-Ep/ID and non-RTT-Ep/ID groups, which might be due to a common (but yet unknown) mechanism of microcephaly. We also found that the regulatory functions of the ghrelin/GH/IGF-1 axis were aberrant in both the RTT-Ep/ID and non-RTT-Ep/ID groups. Further study with a larger sample size should reveal the precise mechanisms controlling the anthropometric and hormonal features in Rett syndrome.

## Acknowledgments

We are grateful to Dr. Masayuki Itoh, National Institute of Neuroscience and Dr. Eiichiro Tanaka, Kurume University School of Medicine for their valuable advice. This work was partly supported by a Grant-in-Aid for Scientific Research (No. 30389283 to M.H., Nos. 22591145 to Y.N. and 21591338 to T.M.) from the Japan Society for the Promotion of Science and research grant from the Ministry of Health, Labor and Welfare of Japan (Intramural Research Grant [21B-5] for Neurological and Psychiatric Disorders of NCNP, and Research on Intractable Diseases 21-110 and 22-133 to T.M.).

## Appendix A. Supplementary data

Supplementary data associated with this article can be found, in the online version, at http://dx.doi.org/10.1016/j.braindev.2013.11.007.

## References

[1] Amir RE, Van den Veyver IB, Wan M, Tran CQ, Francke U, Zoghbi HY. Rett syndrome is caused by mutations in X-linked MECP2, encoding methyl-CpG-binding protein 2. Nat Genet 1999;23:185–8.
[2] Percy AK, Neul JL, Glaze DG, Motil KJ, Skinner SA, Khwaja O, et al. Rett syndrome diagnostic criteria: lessons from the natural history study. Ann Neurol 2010;68:951–5.
[3] Schultz RJ, Glaze DG, Motil KJ, Armstrong DD, del Junco DJ, Hubbard CR, et al. The pattern of growth failure in Rett syndrome. Am J Dis Child 1993;147:633–7.
[4] Oddy WH, Webb KG, Baikie G, Thompson SM, Reilly S, Fyfe SD, et al. Feeding experiences and growth status in a Rett syndrome population. J Pediatr Gastroenterol Nutr 2007;45:582–90.
[5] Tarquino DC, Motil KJ, Hou W, Lee HS, Glaze DG, Skinner SA, et al. Growth failure and outcome in Rett syndrome: specific growth references. Neurology 2012;79:1653–61.
[6] Bebbington A, Percy A, Christodoulou J, Ravine D, Ho G, Jacoby P, et al. Updating the profile of C-terminal MECP2 deletions in Rett syndrome. J Med Genet 2010;47:242–8.
[7] Kojima M, Kangawa K. Ghrelin: structure and function. Physiol Rev 2005;85:495–522.

[8] Jarkovská Z, Rosická M, Marek J, Hána V, Weiss V, Justová V, et al. Plasma levels of total and active ghrelin in acromegaly and growth hormone deficiency. Physiol Res 2006;55:175–81.
[9] Laposky AD, Bass J, Kohsaka A, Turek FW. Sleep and circadian rhythms: key components in the regulation of energy metabolism. FEBS Lett 2008;582:142–51.
[10] Perrini S, Laviola L, Carreira MC, Cignarelli A, Natalicchio A, Giorgino F. The GH/IGF-1 axis and signaling pathways in the muscle and bone: mechanisms underlying age-related skeletal muscle wasting and osteoporosis. J Endocrinol 2010;205:201–10.
[11] Laviola L, Natalicchio A, Perrini S, Giorgino F. Abnormalities of IGF-1 signaling in the pathogenesis of diseases of the bone, brain, and fetoplacental unit in humans. Am J Physiol Endocrinol Metab 2008;295:E991–9.
[12] Le Roith D, Bondy C, Yakar S, Liu JL, Butler A. The somatomedin hypothesis: 2001. Endocr Rev 2001;22:53–74.
[13] Russo VC, Gluckman PD, Feldman EL, Werther GA. The insulin-like growth factor system and its pleiotropic functions in brain. Endocr Rev 2005;26:916–43.
[14] D'Ercole AJ, Ye P. Expanding the mind: insulin-like growth factor 1 and brain development. Endocrinology 2008;149:5958–62.
[15] Sato T, Nakamura Y, Shiimura Y, Ohgusu H, Kangawa K, Kojima M. Structure, regulation and function of ghrelin. J Biochem 2012;151:119–28.
[16] Sato M, Nakahara K, Goto S, Kaiya H, Miyazato M, Date Y, et al. Effects of ghrelin and des-acyl ghrelin on neurogenesis of the rat fetal spinal cord. Biochem Biophys Res Commun 2006;350:598–603.
[17] Tolle V, Bassant MH, Zizzari P, Poindessous-Jazat F, Tomasetto C, Epelbaum J, et al. Ultradian rhythmicity of ghrelin secretion in relation with GH, feeding behavior, and sleep–wake patterns in rats. Endocrinology 2002;143:1353–61.
[18] Van Cauter E, Copinschi G. Interrelationships between growth hormone and sleep. Growth Horm IGF Res 2000;10(Suppl B): S57–62.
[19] Hara M, Nishi Y, Yamashita Y, Yoh J, Takahashi S, Nagamitsu S, et al. Ghrelin levels are reduced in Rett syndrome patients with eating difficulties. Int J Devl Neurosci 2011;29:899–902.
[20] de Oris M, Onyango AW, Borghi E, Garza C, Yang H. Comparison of the world health organization (WHO) child growth standards and the national center for health statistics/ WHO international growth reference: implications for child health programmes. Public Health Nutr 2006;9:942–7.
[21] Hosoda H, Kojima M, Matsuo H, Kangawa K. Ghrelin and des-acyl ghrelin: two major forms of rat ghrelin peptide in gastrointestinal tissue. Biochem Biophys Res Commun 2000;279:909–13.
[22] Yoh J, Nishi Y, Hosoda H, Tajiri Y, Yamada K, Yanase T, et al. Plasma levels of n-decanoyl ghrelin, another acyl- and active-form of ghrelin, in human subjects and the effects of glucose- or meal-ingestion on its dynamics. Regul Pept 2011;167:140–8.
[23] Kojima M, Hosoda H, Date Y, Nakazato M, Matsuo H, Kangawa K. Ghrelin is a growth-hormone-releasing acylated peptide from stomach. Nature 1999;402:656–60.
[24] Issaacs JS, Murdock M, Lane J, Percy AK. Eating difficulties in girls with Rett syndrome compared with other developmental disabilities. J Am Diet Assoc 2003;103:224–30.
[25] Rosman NP, Tarquinio DC, Datseris M, Hou W, Mannheim GB, Emigh CE, et al. Postnatal-onset microcephaly: pathogenesis, pattern of growth, and prediction of outcome. Pediatrics 2011;127:665–71.
[26] Lawson JA, Vogrin S, Bleasel AF, Cook MJ, Burns L, McAnally L, et al. Predictors of hippocampal, cerebral, and cerebellar volume reduction in childhood epilepsy. Epilepsia 2000;41:1540–5.
[27] Kaufmann WE, Moser HW. Dendritic anomalies in disorders associated with mental retardation. Cereb Cortex 2000;10:981–91.
[28] Segawa M. Discussant – pathophysiologies of Rett syndrome. Brain Dev 2001;23(Suppl 1):S218–23.
[29] Kim J, Nakajima K, Oomura Y, Wayner MJ, Sasaki K. Electrophysiological effects of ghrelin on pedunculopontine tegmental neurons in rats: an in vitro study. Peptides 2009;30:745–57.
[30] Motil KJ, Schultz R, Brown B, Glaze DG, Percy AK. Altered energy balance may account for growth failure in Rett syndrome. J Child Neurol 1994;9:315–9.
[31] Camurdan MO, Bideci A, Demirel F, Cinaz P. Serum ghrelin, IGF-1 and IGFBP-3 levels in children with normal variant short stature. Endocr J 2006;53:479–84.
[32] Whatmore AJ, Hall CM, Jones J, Westwood M, Clayton PE. Ghrelin concentrations in healthy children and adolescents. Clin Endocrinol (Oxf) 2003;59:649–54.
[33] Tropea D, Giacometti E, Wilson NR, Beard C, McCurry C, Fu DD, et al. Partial reversal of Rett syndrome-like symptoms in MeCP2 mutant mice. Proc Natl Acad Sci USA 2009;106:2029–34.
[34] Pini G, Scusa MF, Congiu L, Benincasa A, Morescalchi P, Bottiglioni I, et al. IGF-1 as a potential treatment for Rett syndrome: safety assessment in six Rett patients. Autism Res Treat 2012;2012:679801.
[35] Motil KJ, Ellis KJ, Barrish JO, Caeg E, Glaze DG. Bone mineral content and bone mineral density are lower in older than younger females with Rett syndrome. Pediatric Res 2008;64:435–9.
[36] Jefferson AL, Woodhead HJ, Fyfe S, Briody J, Bebbington A, Strauss BJ, et al. Bone mineral content and density in Rett syndrome and their contributing factors. Pediatric Res 2011;69:293–8.
[37] Gil-Campos M, Aquilera CM, Cañete R, Gil A. Ghrelin: a hormone regulating food intake and energy homeostasis. Br J Nutr 2006;96:201–26.
[38] Veldhuis JD, Bowers CY. Integrating GHS into the ghrelin system. Int J Pept 2010;2010:1–41.
[39] Caffarelli C, Gonnelli S, Tanzilli L, Hayek J, Vichi V, Franci MB, et al. The relationship between serum ghrelin and body composition with bone mineral density and QUS parameters in subjects with Rett syndrome. Bone 2012;50:830–5.
[40] Huppke P, Roth C, Christen HJ, Brockmann K, Hanefeld F. Endocrinological study on growth retardation in Rett syndrome. Acta Paediatr 2001;90:1257–61.
[41] Akamizu T, Shinomiya T, Irako T, Fukunaga M, Nakai Y, Nakai Y. Separate measurement of plasma levels of acylated and desacylated ghrelin in healthy subjects using a new direct ELISA assay. J Clin Endocrinol Metab 2005;90:6–9.
[42] Gurdon JB, Bourillot PY. Morphogen gradient interpretation. Nature 2001;413:797–803.
[43] Affolter M, Basler K. The decapentaplegic morphogen gradient: from pattern formation to growth regulation. Nat Rev Genet 2007;8:663–74.
[44] Zachariah RM, Rastegar M. Linking epigenetics to human disease and Rett syndrome: the emerging novel and challenging concepts in MeCP2 research. Neural Plast 2012;2012: 415825.